

## Unusual low-temperature behavior in the half-filled band of the one-dimensional extended Hubbard model in atomic limit

Onofre Rojas <sup>1</sup>, S. M. de Souza,<sup>1</sup> J. Torrico <sup>2</sup>, L. M. Veríssimo <sup>3,4</sup>, M. S. S. Pereira <sup>4</sup>, M. L. Lyra <sup>4</sup> and Oleg Derzhko <sup>5</sup>

<sup>1</sup>*Departamento de Física, Universidade Federal de Lavras, CP 3037, 37200-900 Lavras-MG, Brazil*

<sup>2</sup>*Departamento de Física, Instituto de Ciências Exatas, Universidade Federal de Alfenas, 37133-840 Alfenas, Minas Gerais, Brazil*

<sup>3</sup>*Donostia International Physics Center, Paseo Manuel de Lardizabal 4, E-20018 San Sebastián, Spain*

<sup>4</sup>*Instituto de Física, Universidade Federal de Alagoas, 57072-970 Maceió, Alagoas, Brazil*

<sup>5</sup>*Institute for Condensed Matter Physics, National Academy of Sciences of Ukraine, Svientsitskii Street 1, 79011 L'viv, Ukraine*



(Received 23 March 2024; revised 17 May 2024; accepted 1 August 2024; published 22 August 2024)

Recently, a kind of finite-temperature pseudotransition was observed in several quasi-one-dimensional models. In this work, we consider a genuine one-dimensional extended Hubbard model in the atomic limit, influenced by an external magnetic field and with the arbitrary number of particles controlled by the chemical potential. The one-dimensional extended Hubbard model in the atomic limit was initially studied in the seventies and has been investigated over the past decades, but it still surprises us today with its fascinating properties. We rigorously analyze its low-temperature behavior using the transfer matrix technique and provide accurate numerical results. Our analysis confirms that there is an anomalous behavior in the half-filled band, specifically occurring between the alternating pair (AP) and paramagnetic (PM) phases at zero temperature. Previous investigations did not deeply identify this anomalous behavior, maybe due to the numerical simplicity of the model, but from an analytical point of view this is not so easy to manipulate algebraically because one needs to solve an algebraic cubic equation. In this study, we explore this behavior and clearly distinguish the pseudotransition, which could easily be mistaken with a real phase transition. This anomalous behavior mimics features of both first- and second-order phase transitions. However, due to its nature, we cannot expect a finite-temperature phase transition in this model.

DOI: [10.1103/PhysRevE.110.024130](https://doi.org/10.1103/PhysRevE.110.024130)

### I. INTRODUCTION

Recent studies on various effective one-dimensional models with short-range interactions have revealed intriguing thermal behaviors, resembling first- and second-order phase transitions [1]. This peculiar behavior, to be called further pseudotransition [1], is also dubbed ultranarrow phase crossover [2,3], thermal pseudotransition [4], or curious thermodynamics that resembles a phase transition [5]. Pseudotransitions have been further analyzed in Ref. [6], focusing on spin correlation functions. The simplest models where this unusual behavior arises are in the Ising diamond chain [3,7,8]. Another similar decorated Ising chain discussed is the Ising sawtooth-like chain model [8], along with two- and three-leg Ising ladder models [2,9,10]. Pseudotransitions also appear in other models, such as the Ising-Heisenberg diamond chain [11,12] and the one-dimensional double-tetrahedral model with alternating Ising spins and delocalized electrons [13]. Similar phenomena are observed in ladder models with Ising-Heisenberg coupling [14] and triangular tube models [15], highlighting a pattern of pseudotransition. Further investigations [9,16,17] have shown some kind of universality of power-law exponents, while still satisfying the Rushbrooke inequality. All the above models are related to *classical* and *classical-quantum* spin models; here by classical we mean that the Hamiltonian does not contain noncommuting terms. However, models of other natures, like the extended

Hubbard model in a diamond chain structure [18] and the Potts model on a diamond chain structure, have also exhibited this unusual behavior. On the other hand, exploring pseudotransitions in genuine one-dimensional systems without decoration couplings is rather interesting. In this sense, the Zimm-Bragg-Potts model was recently explored and found to exhibit this anomalous behavior [19].

On the other hand, the Hubbard model [20] stands as a foundational model in the modern theory of strongly correlated electrons, playing a paradigmatic role in the study of electronic correlations in quantum materials. This model is particularly significant in contexts where interactions are crucial. The Bethe ansatz method helps to understand this model better, especially in figuring out how electrons behave in different conditions and how they interact with each other [21]. The one-dimensional extended Hubbard model is a simplified theoretical model that describes the behavior of electrons in a one-dimensional chain, which additionally includes nearest-neighbor interaction energy terms. The nearest-neighbor interaction energy term describes the Coulomb repulsion between electrons occupying neighboring sites. The one-dimensional extended Hubbard model has been widely studied in the literature due to its relevance in understanding the electronic properties of one-dimensional materials such as carbon nanotubes and organic conductors [22]. It also serves as a simple prototype model for studying strongly correlated electron systems [23]. On the

other hand, several theoretical investigations have focused on the extended Hubbard model in the one-dimensional case. Numerous investigations regarding the half-filled ground states of the extended Hubbard model have been conducted. Tsuchiizu and Furusaki [24] revisited the ground-state phase diagram of the one-dimensional half-filled extended Hubbard model, revealing different phases and transitions using a renormalization-group approach. Glocke *et al.* [25] utilized density-matrix renormalization group methods on transfer matrices to study the thermodynamics of the one-dimensional extended Hubbard model at half-filling. This highlights the detection of phase transitions through standard thermodynamic measures like isothermal compressibility and magnetic susceptibility. The study identifies a unique phase with long-range dimer order and delineates the phase diagram, comparing it with quantum Monte Carlo studies [26,27]. The phase diagram and power-law exponents of the one-dimensional  $U - V$  model at quarter-filling were identified using exact diagonalization and various limit results, identifying a transition from Luttinger liquid to charge density wave insulator, noting dominant superconducting or spin density wave fluctuations depending on the value of  $V$  [28]. Further investigation was also performed in Ref. [29].

Recent experiments have successfully demonstrated the realization of an extended fermionic Hubbard model using a two-dimensional lattice composed of dopant-based quantum dots. Quantum dots, often likened to artificial atoms, can be accurately arranged into structures resembling artificial molecules and lattices. These arrangements offer adjustable hopping amplitudes and interaction strengths, as well as the ability to design specific point symmetries. This advancement marks a significant step in the exploration of complex quantum systems and could pave the way for new insights into the behaviors of electronic systems [30]. Recent angle-resolved photoemission spectroscopy (ARPES) studies on the one-dimensional extended Hubbard model, employing bosonization and time-dependent calculations, reveal insights into electron-phonon coupling and interactions in one-dimensional systems [31]. Earlier, Epstein *et al.* [32] discussed the metal-insulator transition of *N*-methyl phenazinium (NMP) tetracyanoquinodimethane (TCNQ) based on the strongly correlated Hubbard model ( $t \ll U$ ). A considerable number of theoretical studies of this model have been undertaken, and many of its properties are now well known. However, this simple model still surprises us with unexpected features, which are the focus in the following sections.

Although the simplest version of the extended Hubbard model has been considerably studied and applied to various physical systems, here we consider a typical one-dimensional extended Hubbard model in the atomic limit (neglecting the hopping term),

$$\mathbf{H} = \sum_{i=1}^N [U \mathbf{n}_{i,\uparrow} \mathbf{n}_{i,\downarrow} + V \mathbf{n}_i \mathbf{n}_{i+1} - \mu (\mathbf{n}_{i,\uparrow} + \mathbf{n}_{i,\downarrow}) - h (\mathbf{n}_{i,\uparrow} - \mathbf{n}_{i,\downarrow})], \quad (1)$$

where  $U$  is the on-site Coulomb interaction,  $V$  is the Coulomb interaction between electrons on the neighboring sites,  $\mu$  is the

chemical potential, and  $\mathbf{n}_{i,\sigma}$  is the corresponding number operator at site  $i$ , with spin  $\sigma = \{\uparrow, \downarrow\}$  and  $\mathbf{n}_i = \mathbf{n}_{i,\uparrow} + \mathbf{n}_{i,\downarrow}$ . And, the last term reports the contribution of external magnetic field  $h$ . Despite its simplicity, the present model still astonishes us by providing further interesting anomalous properties not previously elucidated elsewhere, through careful analysis.

The present work is organized as follows: In Sec. II, we give the thermodynamics of the one-dimensional extended Hubbard model in the atomic limit, identifying each eigenvalue of the cubic root and determining which one is the largest, a topic not previously elucidated. In Sec. III, we analyze a peculiar property in the low-temperature region and explore the anomalous behavior, along with the corresponding region where the main properties undergo significant changes at this anomalous temperature. This phenomenon is what we refer to as the quasi-phase diagram [1]. In Sec. IV, we explore additional physical quantities, reporting the influence of pseudotransition. Finally, in Sec. V, we present our conclusions.

## II. THERMODYNAMICS OF THE MODEL

In the 1970s, the thermodynamics of the one-dimensional extended Hubbard model in the atomic limit garnered significant interest, with pioneering analyses by Bari [33], Beni and Pincus [34], and Gallinar [35] employing the transfer matrix approach. These studies examined specific heat, static magnetic susceptibility, and density-density correlation functions at various temperatures, particularly focusing on the half-filled band and briefly on the quarter-filled band case with infinite intra-atomic Coulomb repulsion. Later, Mancini and Mancini [36,37] advanced this research using Green's function and equations of motion formalism, finding four distinct phases and diverse charge orderings at zero temperature. Their work also considered the influence of external magnetic fields [38] on thermodynamic properties like magnetization and specific heat, identifying critical fields associated with polarization levels.

### A. Transfer matrix

In order to express the transfer matrix of the model, we use the following natural basis  $\{|0\rangle, |\uparrow\rangle, |\downarrow\rangle, |1\rangle\}$ . The first state corresponds to the vacuum state, the second state denotes the spin-up state, the third state is the spin-down state, and the fourth state corresponds to two spins with opposite spins on the same site.

In principle, this model can be solved using the transfer matrix technique [34,39], and the transfer matrix is given by

$$\mathbf{W} = \begin{bmatrix} 1 & yw_{0,1} & y^{-1}w_{0,1} & w_{0,2} \\ yw_{0,1} & y^2w_{1,1} & w_{1,1} & yw_{1,2} \\ y^{-1}w_{0,1} & w_{1,1} & y^{-2}w_{1,1} & y^{-1}w_{1,2} \\ w_{0,2} & yw_{1,2} & y^{-1}w_{1,2} & w_{2,2} \end{bmatrix}, \quad (2)$$

where  $w_{0,1} = e^{\beta\mu/2}$ ,  $w_{0,2} = e^{\beta(\mu-U/2)}$ ,  $w_{1,1} = e^{\beta(\mu-V)}$ ,  $w_{1,2} = e^{\beta(3\mu/2-2V-U/2)}$ ,  $w_{2,2} = e^{\beta(2\mu-4V-U)}$ ,  $y = e^{\beta h/2}$ , and  $\beta$  is the inverse temperature,  $\beta = 1/(k_B T)$ .

Certainly, we can proceed by calculating  $\det(\mathbf{W} - \lambda \mathbf{1}) = 0$  to obtain the eigenvalues of the transfer matrix, as was previously done by Beni and Pincus [34]. Alternatively, we can

manipulate the transfer matrix for convenience, considering the spin inversion symmetry, in order to simplify our perturbative approach calculations later on. Thus, we can employ a new set of basis vectors  $\{|0\rangle, |\uparrow\rangle, |\downarrow\rangle, |\leftrightarrow\rangle\}$ , where  $|\uparrow\rangle = (y|\uparrow\rangle + y^{-1}|\downarrow\rangle)/\sqrt{z}$  corresponds to the symmetric state and  $|\leftrightarrow\rangle = (y|\downarrow\rangle - y^{-1}|\uparrow\rangle)/\sqrt{z}$  denotes the antisymmetric state, with  $z = y^2 + y^{-2} = 2 \cosh(\beta h)$ . Note that these states are invariant under simultaneous spin inversion and magnetic field inversion. In this new basis, the transfer matrix (2) simply becomes

$$\mathbf{W} = \begin{bmatrix} 1 & w_{0,1}\sqrt{z} & w_{0,2} & 0 \\ w_{0,1}\sqrt{z} & w_{1,1}z & w_{1,2}\sqrt{z} & 0 \\ w_{0,2} & w_{1,2}\sqrt{z} & w_{2,2} & 0 \\ 0 & 0 & 0 & 0 \end{bmatrix} = \begin{bmatrix} \mathbf{V} & \mathbf{0} \\ \mathbf{0} & \mathbf{0} \end{bmatrix}, \quad (3)$$

where the matrix  $\mathbf{V}$ , expressed in the basis  $\{|0\rangle, |\uparrow\rangle, |\downarrow\rangle\}$ , results in

$$\mathbf{V} = \begin{bmatrix} 1 & w_{0,1}\sqrt{z} & w_{0,2} \\ w_{0,1}\sqrt{z} & w_{1,1}z & w_{1,2}\sqrt{z} \\ w_{0,2} & w_{1,2}\sqrt{z} & w_{2,2} \end{bmatrix}. \quad (4)$$

Obviously, the eigenvalue corresponding to the state  $|\leftrightarrow\rangle$  is null.

It is straightforward to diagonalize the transfer matrix by solving the determinant equation  $\det(\mathbf{V} - \lambda \mathbf{1}) = 0$ , which leads to the following secular equation:

$$\lambda^3 + a_2\lambda^2 + a_1\lambda + a_0 = 0, \quad (5)$$

where the coefficients result in

$$\begin{aligned} a_0 &= z(w_{1,2}^2 + w_{0,2}^2 w_{1,1} + w_{0,1}^2 w_{2,2}) \\ &\quad - z(w_{1,1} w_{2,2} - 2w_{0,2} w_{0,1} w_{1,2}), \\ a_1 &= z(w_{1,1} + w_{1,1} w_{2,2} - w_{0,1}^2 - w_{1,2}^2) + w_{2,2} - w_{0,2}^2, \\ a_2 &= -1 - z w_{1,1} - w_{2,2}. \end{aligned} \quad (6)$$

Therefore, the roots of the algebraic cubic Eq. (5) can be expressed conveniently using trigonometric function, i.e.,

$$\lambda_j = 2\sqrt{Q} \cos\left(\frac{\phi - 2\pi j}{3}\right) - \frac{1}{3}a_2, \quad j = 0, 1, 2, \quad (7)$$

with

$$\phi = \arccos\left(\frac{R}{\sqrt{Q^3}}\right), \quad (8)$$

$$Q = \frac{a_2^2 - 3a_1}{9}, \quad (9)$$

$$R = \frac{9a_1 a_2 - 27a_0 - 2a_2^3}{54}. \quad (10)$$

Note that it is sufficient to restrict the cubic equation solution without loss of generality to the interval of  $0 < \phi < \pi$ ; thus, the eigenvalues are ordered as follows:  $\lambda_0 > \lambda_1 > \lambda_2$ . This criterion is discussed in more detail in Ref. [18]. To analyze the characteristics of the eigenvalues in the interval  $0 < \phi < \pi$ , after some trigonometric manipulation, we have

$$\sqrt{Q} - \frac{a_2}{3} < \lambda_0 < 2\sqrt{Q} - \frac{a_2}{3}. \quad (11)$$

Obviously  $\lambda_0$  is definitely positive, because  $a_2 < 0$ . Similarly, for the second eigenvalue, we can express

$$-\sqrt{Q} - \frac{a_2}{3} < \lambda_1 < \sqrt{Q} - \frac{a_2}{3}. \quad (12)$$

In this case,  $\lambda_1$  can be positive or negative depending on the Hamiltonian parameters. For the last eigenvalue, the corresponding interval can be expressed as

$$-2\sqrt{Q} - \frac{a_2}{3} < \lambda_2 < -\sqrt{Q} - \frac{a_2}{3}; \quad (13)$$

similarly,  $\lambda_2$  can be positive or negative. Particularly to satisfy  $\lambda_2 < 0$ , the following condition must be met:  $\sqrt{Q} > -\frac{a_2}{3}$ , which implies that  $a_1 < 0$ . It is noteworthy that for other intervals, the arrangement of the cubic root solutions merely exchanges; for details, see Table 2 of Ref. [18].

As said above, the fourth eigenvalue  $\lambda_3$  of the transfer matrix (2) becomes null.

### B. Thermodynamic quantities and correlators

To analyze thermodynamic quantities, we use the grand partition function for a chain consisting of  $N$  sites

$$\Xi(T, \mu, h, N) = \lambda_0^N + \lambda_1^N + \lambda_2^N. \quad (14)$$

Given the hierarchy of the eigenvalues ( $\lambda_0 > \lambda_1 > \lambda_2$ ), one can determine the grand potential per site in the thermodynamic limit  $N \rightarrow \infty$ , which is solely dictated by the largest eigenvalue of the transfer matrix

$$\begin{aligned} \Omega(T, \mu, h) &= -k_B T \lim_{N \rightarrow \infty} \frac{\ln[\Xi(T, \mu, h, N)]}{N} \\ &= -k_B T \ln \lambda_0. \end{aligned} \quad (15)$$

Here, we introduce several useful thermodynamic quantities; all these quantities will be quantified per site. The entropy is calculated as  $\mathcal{S} = -\frac{\partial \Omega}{\partial T}$ ; the enthalpy is given by  $\mathcal{E} = -\frac{\partial \ln(\lambda_0)}{\partial \beta} = k_B T^2 \frac{\partial \ln(\lambda_0)}{\partial T}$ ; analogously, we can obtain specific heat at constant chemical potential  $C = T \frac{\partial \mathcal{S}}{\partial T} = \frac{\partial \mathcal{E}}{\partial T}$  [40]; the magnetization can be expressed as  $M = -\frac{\partial \Omega}{\partial h}$ ; magnetic susceptibility  $\chi = \frac{\partial M}{\partial h}$ ; the electron density  $\rho$  is determined by  $\rho = -\frac{\partial \Omega}{\partial \mu}$ ; and the isothermal compressibility is derived from  $\kappa = \frac{1}{\rho^2} \frac{\partial \rho}{\partial \mu}$ .

It is also feasible to determine other quantities using  $\rho$  and  $M$ , which can be expressed as  $\rho = \langle n_\uparrow \rangle + \langle n_\downarrow \rangle$  and  $M = \langle n_\uparrow \rangle - \langle n_\downarrow \rangle$ , leading to the expressions

$$\langle n_\uparrow \rangle = \frac{\rho + M}{2} \quad \text{and} \quad \langle n_\downarrow \rangle = \frac{\rho - M}{2}. \quad (16)$$

Similarly, we can also obtain the following quantities:

$$\langle n_\uparrow n_\downarrow \rangle = \frac{\partial \Omega}{\partial U}, \quad \langle \mathbf{n}_i \mathbf{n}_{i+1} \rangle = \frac{\partial \Omega}{\partial V}, \quad (17)$$

where we define

$$\langle \mathbf{n}_i \mathbf{n}_{i+1} \rangle \equiv \langle (\mathbf{n}_{i,\uparrow} + \mathbf{n}_{i,\downarrow})(\mathbf{n}_{i+1,\uparrow} + \mathbf{n}_{i+1,\downarrow}) \rangle. \quad (18)$$

Furthermore, for a transfer matrix with a nondegenerate and positively defined spectrum, one can easily define the correlation length  $\xi$  as the inverse logarithm of the ratio of the largest and the second-largest eigenvalue. Although

our transfer matrix eigenvalues spectrum is nondegenerate, some eigenvalues could become negative. Therefore, we need to compare the magnitude of each eigenvalue. For instance, focusing near the pseudotransition, the eigenvalues become  $\lambda_0 > 0$  and, similarly,  $\lambda_1 > 0$  is also positive. Nevertheless,  $\lambda_2 < 0$ . However, in terms of magnitude, we cannot determine whether  $|\lambda_1|$  or  $|\lambda_2|$  is the second largest. Depending on the Hamiltonian parameters, we may have  $|\lambda_1| > |\lambda_2|$  or  $|\lambda_1| < |\lambda_2|$ . Therefore, for our case, we define the correlation length [41,42] as follows:

$$\xi = \left[ \ln \left( \frac{\lambda_0}{\max(|\lambda_1|, |\lambda_2|)} \right) \right]^{-1}. \quad (19)$$

Note that  $\max(|\lambda_1|, |\lambda_2|)$  has nothing to do with exchanging cubic root solutions but depends solely on the Hamiltonian parameters.

Evidently the correlation length  $\xi$  becomes more intricate due to the competition between the magnitudes of the second-largest eigenvalues. This complexity in  $\xi$  is more pronounced near the point where the magnitudes of these eigenvalues compete. Far from this point of competition, the behavior of  $\xi$  could be more straightforwardly described.

### III. PHASE DIAGRAMS

In what follows, we discuss the ground-state energy, focusing on peculiar regions where anomalous behavior appears. Then, we consider the low-temperature case to discuss quasi-phase diagrams and define a peculiar temperature.

#### A. Zero-temperature phase diagram

In the absence of magnetic field  $h$ , the first ground state to consider is the frustrated phase  $\text{FR}_1$ ,

$$|\text{FR}_1\rangle = \bigotimes_{j=1}^{N/2} |0, \sigma_{2j}\rangle \quad \text{or} \quad \bigotimes_{j=1}^{N/2} |\sigma_{2j}, 0\rangle, \quad (20)$$

with the respective ground-state energy

$$E_{\text{FR}_1} = -\frac{h}{2} - \frac{\mu}{2}. \quad (21)$$

Note that the frustrated ground-state energy occurs just at  $h = 0$ . For a non-null magnetic field, the state aligns with the magnetic field, thereby becoming nonfrustrated. The electron density for this phase is given by  $\rho = 1/2$ , commonly known as the quarter-filled band. The residual entropy (per site) of this phase is expressed as  $\mathcal{S} = k_B \ln(2)/2$ .

Another phase is the frustrated phase  $\text{FR}_2$  given by

$$\begin{aligned} |\text{FR}_2\rangle &= \bigotimes_{j=1}^N |\uparrow\rangle, \\ &= \frac{1}{\sqrt{z}^N} \bigotimes_{j=1}^N (y|\uparrow\rangle + y^{-1}|\downarrow\rangle). \end{aligned} \quad (22)$$

The ground-state energy for this phase is

$$E_{\text{FR}_2} = V - h - \mu. \quad (23)$$

Here again, the frustrated ground-state energy occurs only when  $h = 0$ . However, when  $h \neq 0$ , the state gradually aligns with the magnetic field, losing its frustration. The residual entropy of this phase is  $\mathcal{S} = k_B \ln(2)$ , and the particle density is  $\rho = 1$  (half occupancy).

At a half-filling band or electron density  $\rho = 1$ , we observe the alternation pair phase AP

$$|\text{AP}\rangle = \bigotimes_{j=1}^{N/2} |0, \uparrow\rangle \quad \text{or} \quad \bigotimes_{j=1}^{N/2} |\uparrow, 0\rangle. \quad (24)$$

The corresponding ground-state energy is

$$E_{\text{AP}} = \frac{U}{2} - \mu. \quad (25)$$

Notably, the AP phase has no residual entropy and can be identified as a charge-density wave (CDW) [25].

The third frustrated phase  $\text{FR}_3$ , with an electron density of  $\rho = 3/2$ , in the absence of a magnetic field, is described as

$$|\text{FR}_3\rangle = \bigotimes_{j=1}^{N/2} |\uparrow, \sigma_{2j}\rangle \quad \text{or} \quad \bigotimes_{j=1}^{N/2} |\sigma_{2j}, \uparrow\rangle. \quad (26)$$

The ground-state energy for this phase is

$$E_{\text{FR}_3} = \frac{U}{2} + 2V - \frac{h}{2} - \frac{3\mu}{2}. \quad (27)$$

Again, the ground state is frustrated at  $h = 0$ , whereas for  $h \neq 0$  the system loses its frustration. For  $h = 0$ , the corresponding residual entropy leads to  $\mathcal{S} = k_B \ln(2)/2$ .

Lastly, in the fully filled phase FF, the ground state results in

$$|\text{FF}\rangle = \bigotimes_{j=1}^N |\uparrow\rangle. \quad (28)$$

The corresponding ground-state energy is

$$E_{\text{FF}} = U - 4V - 2\mu. \quad (29)$$

The electron density in this phase is  $\rho = 2$ , and there is no residual entropy.

It is important to note that in all the aforementioned states, the magnetization obviously becomes  $M = 0$  at  $h = 0$ . Furthermore, including a magnetic field  $h$  into the phase diagrams generally results in properties similar to those observed in the absence of a magnetic field (not illustrated). The main distinction is that the regions previously identified as frustrated (FR) become unfrustrated in the presence of a magnetic field. An equivalent analysis was earlier performed by Mancini and Mancini [37,38], offering a different perspective on the phase diagram. For example, in the  $\text{FR}_1$  (quarter-filled) and  $\text{FR}_3$  (three-quarter-filled) regions, under a sufficiently strong magnetic field, the spin arrangements align parallel to the external magnetic field. In contrast, the  $\text{FR}_2$  phase, characterized by one particle per site with randomly oriented spins, begins to show alignment under the influence of a magnetic field. As the magnetic field strength increases, the spins start aligning with the external field, transitioning into a fully polarized or paramagnetic phase PM.

For a clearer illustration, we present in Fig. 1 the phase diagram in the  $h/U - \mu/U$  plane for fixed  $V = 0.55$ . Black

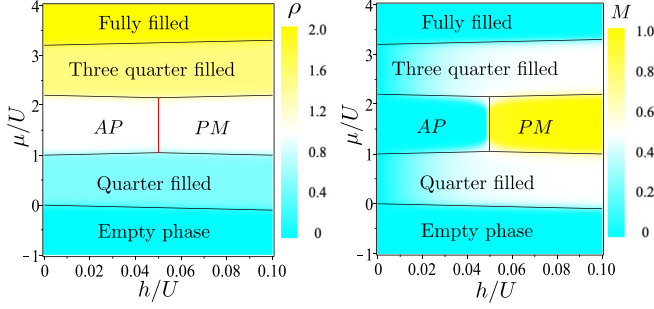


FIG. 1. Phase diagram in the  $\mu/U - h/U$  plane, with solid lines, describes the zero-temperature phase diagram for the fixed  $V = 0.55$ . Meanwhile, the background color density plot corresponds to electron density (left) and magnetization (right), assuming the low temperature  $T = 0.03$ .

solid lines describe the zero-temperature phase diagram, while the red solid line delineates an unusual phase boundary where anomalous behavior emerges. In the same plot, we also incorporate a color density plot corresponding to electron density  $\rho$  (left) and magnetization  $M$  (right) in the low-temperature region  $T = 0.03$ . In the left panel, we observe a phase transition between alternating pair (AP) and paramagnetic (PM) phases in the half-filled region, where a constant density is clearly visible. In contrast, we note a distinct change in magnetization from  $M = 0$  in the AP phase to  $M = 1$  in the PM phase. The half-filling band region will be our focus from now on.

Table I presents the behavior of the phase boundaries. The second column lists the magnetic field  $h$  at each phase boundary, and the fourth column details the residual entropy at the different boundaries. Typically, at the interface between two phases, the residual entropy is higher than in the adjacent phases. However, in Table I, the phase boundary between  $FR_2$  and AP exhibits an unusual behavior: The residual boundary entropy does not exceed the residual entropy of  $FR_2$  [43]. This anomaly leads to unexpected behavior at finite temperatures, as discussed in Sec. III B.

The phase diagram in the  $U - V$  plane, assuming a zero magnetic field and considering a suitable chemical potential ( $\mu = 1.58$ ) to enhance the anomalous behavior at a half-filled band, is illustrated in Fig. 2. This phase diagram features a fully filled band phase FF, an alternating pair phase AP, and

TABLE I. The second column provides zero-temperature phase boundary conditions, the third column gives the chemical potential at the phase boundary, while the fourth column reports the associated residual boundary entropy. Note that for the  $FR_2 - AP$  there is no dependence on  $\mu$  according to the second column, and therefore the corresponding row in the third column is empty.

Boundary	$h$	$\mu$	$S/k_B$
FF - $FR_3$	$\mu - U - 2V$	$h + U + 2V$	$\ln(2)$
$FR_3 - AP$	$4V - \mu$	$4V - h$	$\ln(3)/2$
$FR_3 - FR_2$	$\mu - U - 4V$	$h + U + 4V$	$\ln(1 + \sqrt{3})$
$FR_2 - AP$	$V - \frac{U}{2}$		$\ln(2)$
$FR_1 - AP$	$\mu - U$	$\mu + U$	$\ln(3)/2$
$FR_1 - FR_2$	$2V - \mu$	$2V - h$	$\ln(1 + \sqrt{3})$

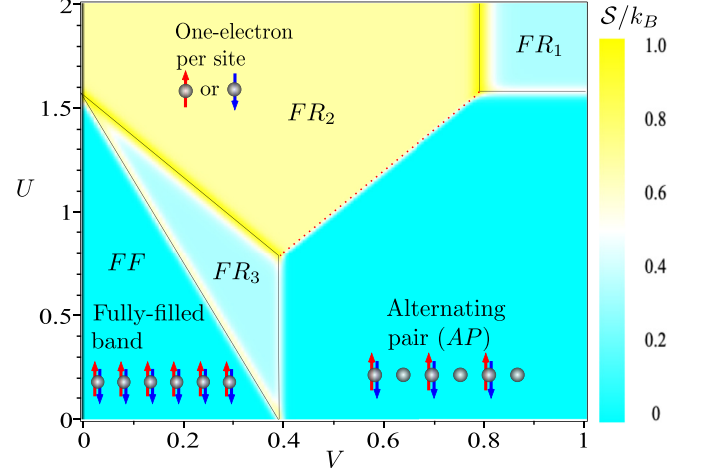


FIG. 2. Phase diagram in the  $U - V$  plane under the assumption of zero magnetic field and  $\mu = 1.58$ . The solid line represents the phase diagram at zero temperature, while the background density plot illustrates the entropy at  $T = 0.01$ .

three frustrated phases. The first frustrated phase  $FR_1$  corresponds to a quarter-filled band of electrons, with spins that can point either up or down, an electron density of  $\rho = 1/2$ , and a residual entropy of  $S = k_B \ln(2)/2$ . In the half-filled region, there is another frustrated phase  $FR_2$  with one electron per site and spins that can also randomly point up or down, having a residual entropy of  $S = k_B \ln(2)$ . The third frustrated phase  $FR_3$  corresponds to a 3/4-filled band of electrons or a quarter-filled band of holes, with an electron density of  $\rho = 3/2$  and a residual entropy of  $S = k_B \ln(2)/2$ . Additionally, the diagram shows a fully filled band of electrons. All these curves can be obtained from Table I, second column, assuming  $h = 0$ . Solid lines delineate standard phase boundaries, while the dashed line indicates an anomalous boundary between two half-filled regions.

### B. Anomalous behavior in low-temperature region and quasi-phase diagram

In our exhaustive analysis, we explore a unique property emerging in the low-temperature region, a phenomenon not extensively observed or detailed in previous studies [33–35,37,38]. Remarkably, our findings reveal intriguing phenomena within such a simplistic model.

The background of Fig. 2 presents a density plot of entropy in the  $V - U$  plane at a low temperature ( $T = 0.01$ ). Our focus is on the zero-temperature boundary between the  $FR_2$  phase and the AP phase. Given the absence of true phase transitions, with only crossover lines occurring at finite temperatures, we refer to the zero-temperature phases at finite temperatures as quasi-phases. In this low-temperature region, these phases are termed the quasi-frustrated  $qFR_2$  region and the quasi-alternating pair  $qAP$  region or quasi-CDW region, where the arrangement of most spins remains similar to their configurations at zero temperature.

Another perspective of the background density plot illustrating the entropy, as depicted in Fig. 2, can be seen in Fig. 3 for fixed values of  $U = 1$  and  $\mu = 1.58$ , plotted

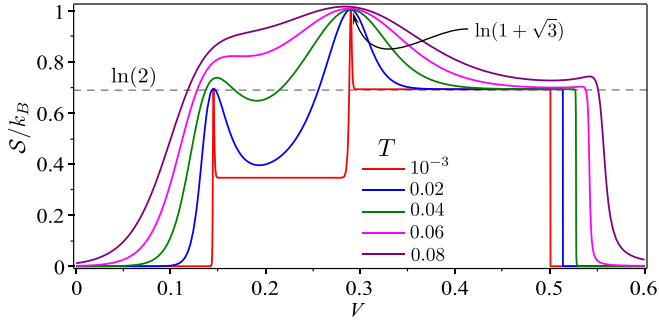


FIG. 3. Entropy as a function of  $V$  for several values of low temperatures, assuming fixed  $U = 1$  and  $\mu = 1.58$ .

against  $V$ . Here, it is evident how residual entropy influences thermal entropy. The peaks at  $V \approx 0.145$  and  $V \approx 0.29$  correspond to the standard interphases between  $\text{FF} - \text{FR}_3$  [with  $\mathcal{S} = k_B \ln(2)$ ] and  $\text{FR}_3 - \text{FR}_2$  [with  $\mathcal{S} = k_B \ln(1 + \sqrt{3})$ ], respectively. However, in the interphase between  $\text{FR}_2 - \text{AP}$  occurring at  $V = 0.5$ , no peaks are observed, indicating anomalous behavior. Here, residual entropy leads to  $\mathcal{S} = k_B \ln(2)$ .

Further evidence of this anomaly is explored in Fig. 4. Figure 4(a) presents the entropy ( $\mathcal{S}$ ) as a function of temperature ( $T$ ) for several values of the external magnetic field, as indicated within the panel. Here, one can clearly observe a swift change in entropy at a specific low-temperature region. Similarly, in Fig. 4(b), we illustrate the magnetization ( $M$ ) as a function of temperature ( $T$ ); the colored curves refer to the same set of parameters as in Fig. 4(a). Once again, we observe that the magnetization for all sets of parameters is essentially null up to a certain temperature, where an unusual

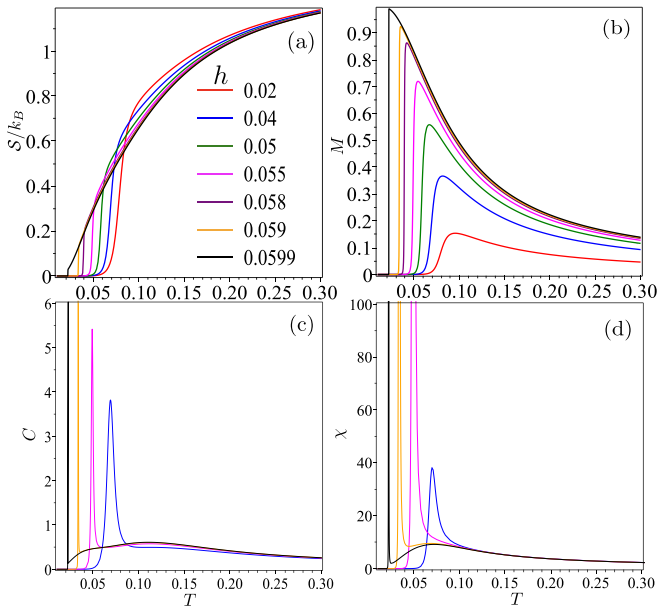


FIG. 4. (a) Entropy against  $T$  for several values of magnetic fields, assuming  $U = 1$  and  $V = 0.56$ . (b) Magnetization as a function of  $T$ . (c) Specific heat as a function of  $T$ . (d) Magnetic susceptibility as a function of  $T$ . All curves correspond to the legend given in (a).

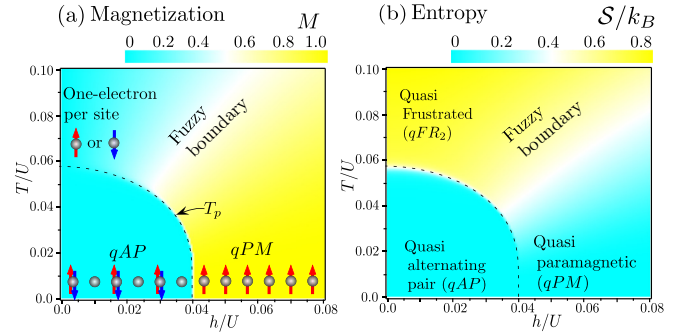


FIG. 5. Quasi-phase diagram depicting the half-filled band in the  $h/U - T/U$  plane, with fixed parameters  $V/U = 0.54$  and  $\mu/U = 1.58$ . The dashed curve delineates the peculiar temperature  $T_p$ . (a) and (b) Density plots of magnetization and entropy, respectively.

feature arises, followed by a rapid change in magnetization. Almost full polarization is achieved above the anomalous temperature with increasing magnetic fields. For moderately high temperatures, standard thermal magnetization governs. Another quantity we examine is the specific heat as a function of temperature under the same conditions as in Fig. 4(a). Here, one can clearly observe very sharp peaks, with the sharpness increasing at lower temperatures, akin to a second-order phase transition, although it is merely a sharp peak with no divergence. The magnetic susceptibility as a function of temperature is depicted in Fig. 4(d), where we also observe a very sharp peak at a certain temperature. Although it mimics a second-order phase transition, there is no divergence that would indicate a genuine phase transition. Therefore, we will refer to these anomalous peaks as a “false” phase transition or pseudotransition at a finite temperature.

In exploring another intriguing aspect of the low-temperature region, Fig. 5(a) presents a density plot of magnetization  $M$  in the  $h/U - T/U$  plane, assuming  $V/U = 0.54$  and  $\mu/U = 1.58$ . Here, the dashed line represents the peculiar temperature  $T_p$ . Below a magnetic field of  $h/U = 0.04$  at sufficiently low temperatures, the system resides in a quasi alternating-pair  $qAP$  region, characterized by particles predominantly arranged in alternating pairs. As the magnetic field increases within this low-temperature regime, the system goes swiftly into a quasi-paramagnetic  $qPM$  region, where most spins, one per site, align parallel to the magnetic field. Conversely, at very weak magnetic fields and increasing temperatures, the  $\text{FR}_2$  frustrated system leads into a quasi-frustrated  $qFR_2$  region. The boundary between  $qFR_2$  and  $qPM$  is marked by a standard crossover, or as visualized in the magnetization plot, a diffuse boundary, appearing as a fuzzy region. In Fig. 5(a), one can observe the magnetization shift between  $qAP$  and  $qPM$  regions, although the boundary between  $qAP$  and  $qFR_2$  remains indistinct due to null magnetization in both regions. Similarly, Fig. 5(b) displays the entropy  $\mathcal{S}$ , using the same parameters as Fig. 5(a). Here, the crossover boundary, denoted by a dashed line, outlines the peculiar temperature as a function of magnetic field. In contrast, Fig. 5(b) shows that the boundary between  $qAP$  and  $qPM$  becomes indistinguishable with almost null entropy, while the boundary between  $qAP$  and  $qFR_2$  is sharply defined.

This distinction is due to the residual entropy of FR<sub>2</sub> being  $\mathcal{S} = k_B \ln(2)$ . However, at temperatures above  $T > 0.06$ , the entropy significantly increases, becoming clearly larger than  $\mathcal{S} \gtrsim 0.7k_B$ .

### C. Peculiar temperature condition

This detailed analysis further explores the interesting behavior in the low-temperature region of the model. Previously, the peculiar temperature was defined for models where the free energy involved a simple square root expression [1,6,16]. Defining the peculiar temperature generally poses a challenge, as the only available indicator is an anomalous behavior in the low-temperature region, marked by significant changes in entropy and magnetization, along with sharp peaks in correlation length, specific heat, and magnetic susceptibility. At very low temperatures, these peaks occur at roughly the same temperature. However, as the anomalous behavior shifts to higher temperatures  $T_p$ , these peaks appear at slightly different temperatures for each quantity, complicating the definition of the peculiar temperature.

An interesting observation is that this anomalous behavior is evident in fundamental quantities such as the ratio between the second-largest and the largest eigenvalues. To analyze this more deeply, consider the temperature and magnetic field dependence of the eigenvalues. At a fixed magnetic field  $h_1$ , there exists a special temperature, the peculiar temperature  $T_p$ , which satisfies the relation

$$\left. \frac{\partial}{\partial T} \left( \frac{\lambda_1(T, h_1)}{\lambda_0(T, h_1)} \right) \right|_{T_p} = 0. \quad (30)$$

A similar analysis can be conducted by taking derivatives with respect to the magnetic field of the ratio of the second-largest to the largest eigenvalues, assuming a fixed temperature  $T_{p^*}$ :

$$\left. \frac{\partial}{\partial h} \left( \frac{\lambda_1(T_{p^*}, h)}{\lambda_0(T_{p^*}, h)} \right) \right|_{h_1} = 0. \quad (31)$$

Comparing  $T_{p^*}$  and  $T_p$ , we observe that this quantity becomes slightly different as the temperature increases.

In order to explore further properties of the eigenvalues given in (7), let us define  $\hat{\lambda}_j(T, h) = \lambda_j e^{\varepsilon_0(h)/k_B T}$ , where  $\varepsilon_0(h)$  represents the ground-state energy. This formulation, as discussed in Ref. [44], primarily aims to handle the ground-state energy explicitly, thereby circumventing the issue of dealing with extremely large numbers. Thus, Fig. 6(a) depicts the three eigenvalues  $\hat{\lambda}_j$  as functions of temperature, under the conditions of a null magnetic field,  $\mu = 1.58$ ,  $U = 1$ , and  $V = 0.55$ . Below the temperature  $T_1$ ,  $\hat{\lambda}_2$  approaches  $-\hat{\lambda}_0$ , whereas above  $T_1$ ,  $\hat{\lambda}_2$  approaches  $-\hat{\lambda}_1$  but quickly diverges due to thermal fluctuations.

Following this, we introduce the function

$$g(T, h) = \hat{\lambda}_0(T, h) + \hat{\lambda}_1(T, h) + 2\hat{\lambda}_2(T, h). \quad (32)$$

This function,  $g(T, h)$ , can yield either positive or negative values. Therefore, the condition

$$g(T_1, h_1) = 0 \quad (33)$$

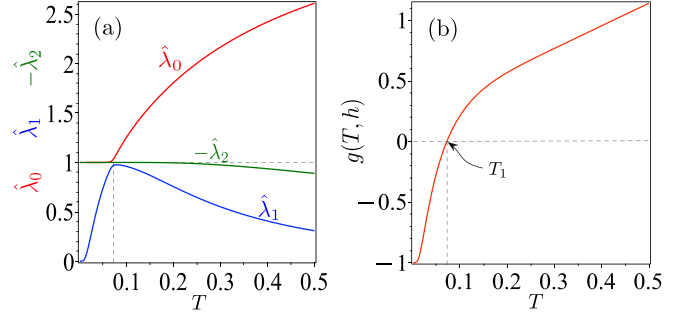


FIG. 6. (a) Cubic root solutions  $\hat{\lambda}_j$  as a function of temperature, under the condition of a null magnetic field ( $h = 0$ ), with fixed values of chemical potential ( $\mu = 1.58$ ), on-site interaction strength ( $U = 1$ ), and nearest-neighbor interaction strength ( $V = 0.55$ ). (b) Plot of  $g(T, 0)$  against temperature  $T$ , using the same parameter set as in (a).

for a fixed  $h_1$  leads to the identification of a specific temperature,  $T_1$ . This approach provides a practical method for examining the temperature-dependent behavior of the system under study.

Figure 6(b) illustrates the function  $g(T, h)$  as it varies with temperature, under the conditions of a null magnetic field,  $\mu = 1.58$ ,  $U = 1$ , and  $V = 0.55$ . In this representation, one can observe that the function  $g(T, h)$  passes through zero at a specific temperature, denoted as  $T_1$ . This provides a clear visual indication of the peculiar point in the behavior of the system.

Alternatively, the condition (33) can be simplified through some algebraic manipulation, even in more general cases and with generic coefficients of a cubic polynomial as outlined in (5). This leads to a simple yet interesting result:

$$2\tilde{a}_2^3 + \tilde{a}_1\tilde{a}_2 + \tilde{a}_0 = 0, \quad (34)$$

where  $\tilde{a}_j$  is defined as  $a_j(T_1, h_1)$ .

Furthermore, we can use the expressions defined in (6) within the context provided by (34) to obtain, after some algebraic manipulation, the following condition:

$$z^2 w_{1,1}^2 + 3z w_{1,1} - w_{0,2}^2 + 2 = 0. \quad (35)$$

Given that  $z w_{1,1} \sim w_{0,2} \gg 1$ , the dominant terms are  $z^2 w_{1,1}^2$  and  $w_{0,2}^2$ , while linear term  $3z w_{1,1}$  and 2 become negligible and are thus omitted for simplification. Consequently, the above expression reduces simply to

$$w_{1,1} z - w_{0,2} = 0. \quad (36)$$

Furthermore, by employing a perturbative approach, as elaborated in the Appendix and illustrated through Eqs. (A3) and (A4) for the unperturbed result, we reaffirm the condition of the equation derived earlier, simplifying our findings into this coherent expression.

In regions of low temperature,  $T_p \approx T_{p^*} \approx T_1$ , which are very close to each other. When this occurs, we can observe anomalous behavior, and we simply define it as the peculiar temperature  $T_p$ .

For the present model the condition (36) provides a sufficiently accurate condition for determining the peculiar temperature, where  $T_p \approx T_1$  holds. Specifically, the peculiar temperature for a fixed magnetic field  $h_1$  can be represented

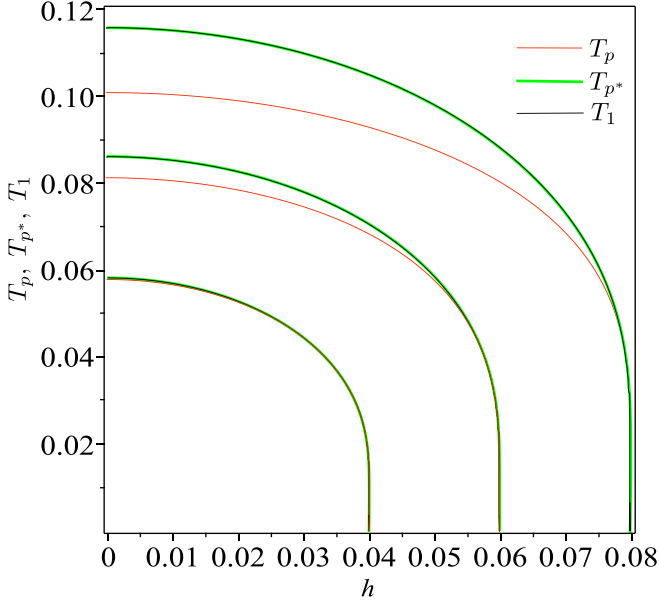


FIG. 7. Plot of  $T_1$  (thin black line),  $T_{p^*}$  (thick green line), and  $T_p$  (thin red line) as functions of  $h$ . The curves are obtained under the assumption of fixed parameters  $\mu = 1.58$ ,  $U = 1$ , and varying  $V$  values:  $V = 0.54$  (inner curve),  $V = 0.56$  (middle curve), and  $V = 0.58$  (outer curve).

using the results  $w_{0,2} = e^{\beta(\mu-U/2)}$ ,  $w_{1,1} = e^{\beta(\mu-V)}$ , and  $z = 2 \cosh(\beta h)$ , leading to the condition

$$2 \cosh(\beta_1 h_1) = e^{\beta_1(V-U/2)}. \quad (37)$$

Assuming  $h_1 > 0$  and at very low temperatures, we deduce that  $h_1 = V - \frac{U}{2}$ . Under these conditions, a pseudotransition is observed at low temperatures.

Eventually, to refine our previous result, we can apply a first-order perturbation approximation with respect to the non-half-filled contribution, as detailed in the Appendix. By using the results given in Eqs. (A9) and (A10), we arrive at the modified condition:

$$w_{1,1}z - w_{0,2} + \frac{3}{2}(1 + w_{2,2}) = 0. \quad (38)$$

Moreover, further corrections can be applied up to a second-order approximation, as detailed in the Appendix.

In Fig. 7, the temperatures  $T_1$  (represented by a thin black line),  $T_{p^*}$  (depicted by a thick green line), and  $T_p$  (illustrated with a thin red line) are shown as functions of  $h$ , under fixed parameters  $\mu = 1.58$ ,  $U = 1$ , and varying  $V$  values: 0.54 (inner curve), 0.56 (middle curve), and 0.58 (outer curve). For the inner curve,  $T_1$ ,  $T_{p^*}$ , and  $T_p$  are visually almost overlapping. However, as we observe the middle curve, the discrepancy between  $T_1 \approx T_{p^*}$  and  $T_p$  becomes more pronounced at higher temperatures. This discrepancy is even more significant for the outer curve. Based on this discrepancy, we can conclude that the peculiar transition is marked for temperatures below  $T_p \lesssim 0.06$ , where all curves overlap (when  $T_1 \approx T_{p^*}$  and  $T_p$  start to diverge). A practical approach to observe the peculiar temperature at higher temperatures is to consider when  $\Delta T_p = T_p - T_{p^*} \rightarrow 0$ . This is because when  $\Delta T_p$  becomes significant, it becomes less meaningful to refer to it as a peculiar temperature.

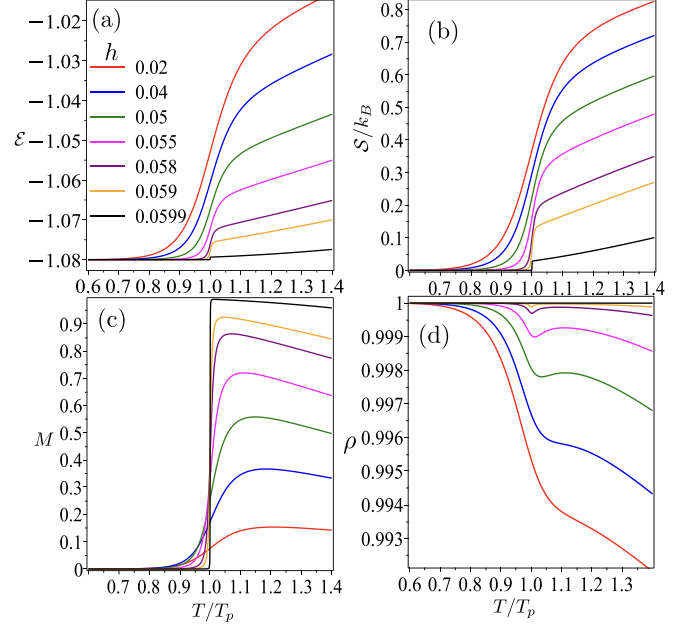


FIG. 8. (a) Enthalpy plotted against  $T/T_p$  for various  $T_p$  values and magnetic fields as specified in Table II, assuming  $U = 1$  and  $V = 0.56$ . (b) Entropy shown as a function of  $T/T_p$ . (c) Magnetization represented as a function of  $T/T_p$ . (d) Electron density depicted as a function of  $T/T_p$ .

#### IV. FURTHER PHYSICAL QUANTITIES

Overall, physical quantities such as magnetic susceptibility or specific heat play fundamental roles in thermodynamics, which are essential for understanding the behavior of the Hubbard model. Therefore, we explore these physical quantities, focusing particularly on the anomalous properties they exhibit.

To provide a clearer depiction of this anomaly, we divide the temperature  $T$  by the peculiar temperature  $T_p$  listed in Table II, where the anomaly manifests. Thus, in Fig. 8(a), the enthalpy  $\mathcal{E}$  is presented as a function of temperature normalized by the peculiar temperature ( $T/T_p$ ) for various fixed magnetic fields, as described within the panel. For each fixed magnetic field, a corresponding peculiar temperature  $T_p$  is given in Table II. At a magnetic field of  $h = 0.0599$ , the enthalpy  $\mathcal{E}$  remains almost constant, but there is a noticeable “jump” at  $T/T_p = 1$ . This indicates a change from the quasi-alternating pair qAP region to a one-electron-per-site region (almost polarized region) or simply a quasi-paramagnetic qPM region. As the external magnetic field decreases, this sharp boundary becomes more gradual, although the “jump” in enthalpy becomes larger. Similarly, in Fig. 8(b), the entropy is observed under the same conditions as in Fig. 8(a), highlighting these features. Notably, for a magnetic field  $h \lesssim 0.06$ , the boundary between qAP and qPM regions becomes more distinct. As  $h$  approaches 0.06, this characteristic resembles a first-order or discontinuous phase transition, despite the absence of actual discontinuity. Figure 8(c) depicts the magnetization  $M$  as a function of  $T/T_p$ . This allows for the corroboration of the spin orientation in the qAP region, where the magnetization is nearly null, while in the qPM region,

TABLE II. Peculiar temperature for  $\mu = 1.58$ ,  $U = 1$ , and  $V = 0.56$ . The second column is computed using Eq. (30), the third column utilizes Eq. (31), and the fourth column is determined by employing Eq. (33).

$h$	$T_p$	$T_{p^*}$	$T_1$
0.020	0.078 915 101 328 2	0.083 114 911 512 3	0.083 131 646 791 6
0.040	0.068 880 694 156 8	0.071 119 937 000 0	0.071 127 747 147 2
0.050	0.058 243 509 164 6	0.059 124 204 425 5	0.059 126 704 736 3
0.055	0.048 934 257 149 1	0.049 208 072 655 5	0.049 208 072 655 5
0.058	0.039 245 973 681 2	0.039 291 366 939 7	0.039 291 439 519 89
0.059	0.033 681 108 445 7	0.033 691 484 433 1	0.033 691 496 636 55
0.0599	0.022 185 975 836 5	0.022 186 033 413 4	0.022 186 033 431 18

the magnetization is almost saturated. This feature is more pronounced at weaker magnetic fields, becoming smoother as the magnetic field decreases. Finally, Fig. 8(d) illustrates the electron density  $\rho$  as a function of  $T/T_p$ , using the same set of magnetic fields considered in Fig. 8(a). Here, it is observed that the electron density remains almost constant  $\rho \approx 1$  (but always smaller than 1,  $\rho < 1$ ) for temperatures  $T/T_p < 1$ , corresponding to a half-filled band. At  $T/T_p = 1$ , there is a small but distinct depression in electron density, which is sharper and more pronounced at higher magnetic fields. As expected, for lower magnetic fields, the electron density decreases with increasing temperature.

In Fig. 9(a), the correlation length  $\xi$  is illustrated as a function of  $T/T_p$  for a fixed external magnetic field, as specified inside the panel. It is important to note that for each fixed magnetic field, there is a corresponding peculiar temperature  $T_p$ , as listed in Table II. The correlation length  $\xi$  [defined in Sec. II B, Eq. (19), and represented by solid lines] demonstrates a

decreasing function with an inflection point around  $T/T_p = 1$ . As the magnetic field decreases, the inflection curvature vanishes. Contrary to what has been previously reported in the literature [1,16,18,43,44],  $\xi$  does not show the typical peak observed around the pseudotransition [1,16,18,43,44]. However, the function  $1/\ln(\lambda_0/\lambda_1)$  (depicted by dashed lines) exhibits a sharp peak as it approaches  $h = 0.06$  at  $T/T_p = 1$ . The peak of this function mimics a typical peak of  $\xi$  around the pseudotransition found in Refs. [1,16,18,43,44], indicative of a swift change between qAP and qPM regions. However, as the magnetic field is decreased, this sharp peak becomes more gradual. Similarly, Fig. 9(b) also illustrates the specific heat  $C$  as a function of  $T/T_p$ , using the same set of magnetic fields. Here, we can observe a sharp peak, akin to that seen in a second-order phase transition, although there is no actual divergence. Furthermore, Fig. 9(c) displays the magnetic susceptibility plotted against  $T/T_p$ , clearly showing the sharp peak at  $T/T_p = 1$ , which mimics a second-order phase transition. Finally, Fig. 9(d) demonstrates the behavior of isothermal compressibility  $\kappa$ . As  $h$  approaches 0.06,  $\kappa$  diminishes, indicating that the system becomes less compressible under these conditions. Conversely, for smaller magnetic fields,  $\kappa$  increases, suggesting that the system is more easily compressible. At relatively low magnetic fields,  $\kappa$  exhibits a minor peak with a maximum at  $T/T_p = 1$ , though this peak becomes less pronounced with lower magnetic fields.

It is worth mentioning that such a quantity as the entropy always tends to increase as  $T$  grows, in accordance with the second law of thermodynamics, which indicates the thermal stability of the system. Similarly, the positivity of specific heat and isothermal compressibility around anomalous behavior also serves as an indicator of stability.

In Fig. 10(a), the spin-up electron density  $\langle n_\uparrow \rangle$  is illustrated as a function of temperature  $T/T_p$  for several weak magnetic fields. Notably, in the half-filled band condition, it is clear how the spin-up averages are organized: For  $T/T_p < 1$ , the spin-up average alternates, given by  $\langle n_\uparrow \rangle \approx 0.5$ , with the remaining spins arranged as spin-down. For  $T/T_p > 1$ , most spins are upwardly arranged. The higher the magnetic field (but  $h < 0.6$ ), the stronger the curvature change at  $T/T_p = 1$ . Similarly, in Fig. 10(b), the spin-down electron density  $\langle n_\downarrow \rangle$  is reported as a function of temperature  $T/T_p$ , for the same set of magnetic fields as in Fig. 10(a). Here, for  $T/T_p < 1$ , almost half of the spins are arranged with spin-down on average, while the remaining are spin-up, as illustrated in Fig. 10(a). In contrast, for  $T/T_p > 1$ , there are nearly no spin-up electrons, as most spins align with the external magnetic field. Another

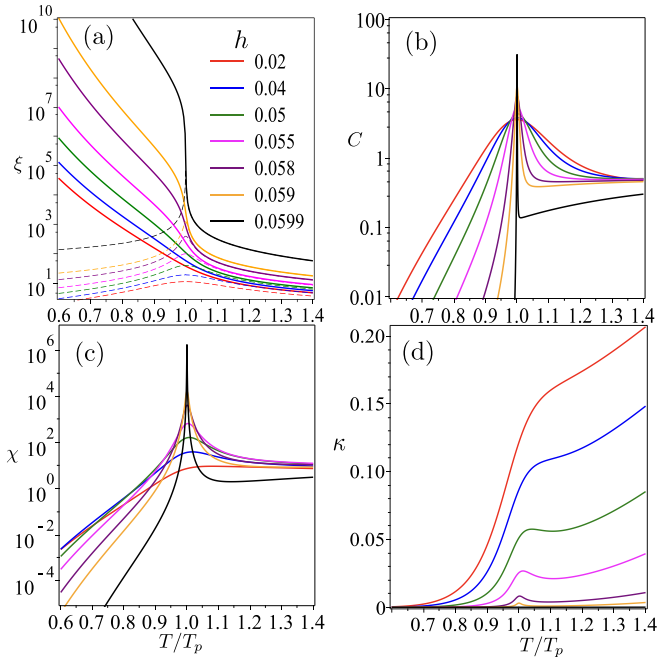


FIG. 9. (a) Correlation length plotted against  $T/T_p$ , with  $T_p$  values provided in Table II, assuming  $U = 1$  and  $V = 0.56$ . Dashed lines describe the function  $1/\ln(\lambda_0/\lambda_1)$ . (b) Specific heat variation with  $T/T_p$ . (c) Magnetic susceptibility vs  $T/T_p$ . (d) Isothermal electron compressibility as a function of  $T/T_p$ .

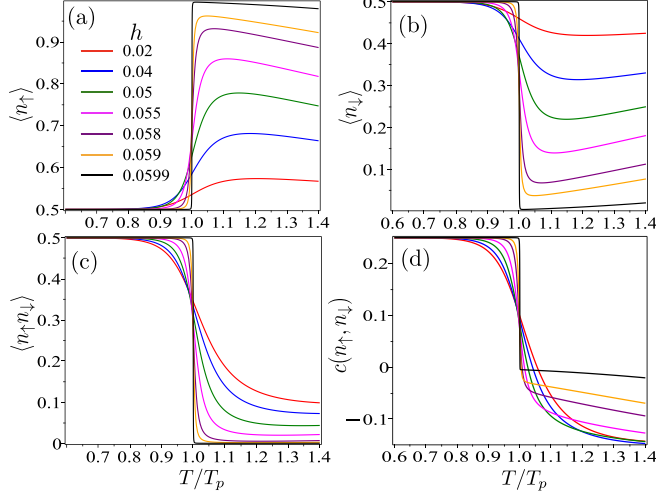


FIG. 10. (a) Electron density for spin-up  $\langle n_{\uparrow} \rangle$  as a function of temperature  $T/T_p$  across various weak magnetic fields, assuming  $U = 1$  and  $V = 0.56$ . (b) Electron density for spin-down  $\langle n_{\downarrow} \rangle$  as a function of temperature  $T/T_p$ , corresponding to the magnetic fields used in (a). (c) On-site average  $\langle n_{\uparrow} n_{\downarrow} \rangle$  as a function of temperature  $T/T_p$ , assuming the magnetic field values from (a). (d) On-site correlation function  $c(n_{\uparrow}, n_{\downarrow})$  as a function of temperature  $T/T_p$  for the same set of parameters as in (a).

interesting quantity is the on-site electron average  $\langle n_{\uparrow} n_{\downarrow} \rangle$  as a function of temperature  $T/T_p$ , assuming the same magnetic field values as in Fig. 10(a). This confirms the electron arrangement in the low-temperature region: For  $T/T_p < 1$ , the average leads to  $\langle n_{\uparrow} n_{\downarrow} \rangle \approx 0.5$ , indicating that most spins are arranged in pairs alternating with empty sites. For  $T/T_p > 1$ ,  $\langle n_{\uparrow} n_{\downarrow} \rangle \rightarrow 0$ , as most spins are parallel and aligned with the external magnetic field. For a very weak magnetic field, the curvature change is evident, and it diminishes as the magnetic field increases. Similarly, in Fig. 10(d), the correlation function  $c(n_{\uparrow}, n_{\downarrow}) = \langle n_{\uparrow} n_{\downarrow} \rangle - \langle n_{\uparrow} \rangle \langle n_{\downarrow} \rangle$  is depicted as a function of temperature  $T/T_p$ , again for the same set of parameters as in Fig. 10(a). For  $T/T_p < 1$ , the correlation function is roughly  $c(n_{\uparrow}, n_{\downarrow}) = 0.25$ , while for  $T/T_p > 1$ , it becomes negative, as  $\langle n_{\uparrow} n_{\downarrow} \rangle \approx 0$ ,  $\langle n_{\uparrow} \rangle \approx 0.5$ , and  $\langle n_{\downarrow} \rangle \approx 0.5$ , leading to a negative correlation function of approximately  $-0.25$ .

## V. CONCLUSION

Our study has provided a comprehensive re-examination of the one-dimensional extended Hubbard model in the atomic limit, a subject initially explored in the 1970s. This result not only confirms previous outcomes of the model but also reveals other insights, especially the occurrence of finite-temperature pseudotransitions in specific quasi-one-dimensional models.

Initially, our analysis focused on delineating the zero-temperature phase diagram at zero magnetic field. Here, we identified three distinct types of frustrated phases, enriching our understanding of the intricate phase structure within the model. This phase characterization was facilitated by the employment of the transfer matrix technique, followed by precise numerical analyses, which unveiled anomalous behaviors within the half-filled band of the model. These

behaviors are particularly pronounced in the low-temperature regime, especially during the gradual shift between AP and PM phases. The subtlety of these anomalous behaviors was possibly overlooked in earlier studies due to the deceptively simple numerical facade of the model, but from an algebraic perspective, requiring the solution of an algebraic cubic equation introduces a level of slightly more elaborate manipulation, revealing the intricate nature of the model.

Further investigations explored the low-temperature pseudophase transitions at the half-filling band, where the aforementioned anomalous behavior is predominantly observed. We observed that close to this anomalous region, a pseudotransition emerges that exhibits characteristics reminiscent of both first- and second-order phase transitions. This pseudotransition is particularly fascinating, as it mimics the intricacies of real phase transitions, adding a layer of sophistication to our understanding of the model. Moreover, our exploration extended to diverse properties such as electron density, on-site correlations, and nearest-site electron averages. In examining these quantities, we discerned the underlying reasons for the occurrence of pseudotransitions, thereby deepening our grasp of the model behavior. The intrinsic nature of the model, defined by its nearest-neighbor interaction, precludes the occurrence of real phase transitions at finite temperatures, thereby accentuating the distinctive properties and behaviors inherent to the model within a low-dimensional system and underscoring its peculiarity.

The property we have explored may not necessarily be exclusive to one-dimensional models; however, uncovering this anomalous residual boundary entropy could become a challenging task in higher-dimensional systems.

## ACKNOWLEDGMENTS

O.R. and S.M.S. thank CNPq and FAPEMIG for partial financial support. M.L.L. and M.S.S.P. also acknowledge the financial support of FAPEAL. O.D. acknowledges support through EURIZON Project No. 3025, which is funded by the European Union under Grant Agreement No. 871072. L.M.V. acknowledges the support of Donostia International Physics Center and iKur estrategia.

## APPENDIX: TRANSFER MATRIX AROUND PSEUDOTRANSITION

The phenomenon of pseudotransition arises near the AP and PM phases. Although the solution of (7) is exact and analytic, the analytical expression for finding the peculiar temperature becomes a cumbersome task due to involving cubic root expression. An alternative approach to determine this condition is to split the transfer matrix into two terms, namely,  $\mathbf{V} = \mathbf{V}_0 + \zeta \mathbf{V}_1$ . Here,  $\mathbf{V}_0$  represents the core structure matrix, whose matrix elements just include the half-filled case, while  $\zeta \mathbf{V}_1$  describes a small perturbation applied to the matrix, corresponding to the non-half-filled band. The detailed formulations of these matrices are provided as follows:

$$\mathbf{V}_0 = \begin{bmatrix} 0 & 0 & w_{0,2} \\ 0 & w_{1,1}\zeta & 0 \\ w_{0,2} & 0 & 0 \end{bmatrix} \quad (\text{A1})$$

and

$$\mathbf{V}_1 = \begin{bmatrix} 1 & w_{0,1}\sqrt{z} & 0 \\ w_{0,1}\sqrt{z} & 0 & w_{1,2}\sqrt{z} \\ 0 & w_{1,2}\sqrt{z} & w_{2,2} \end{bmatrix}, \quad (\text{A2})$$

respectively. In this context,  $\zeta$  acts as a small formal parameter that, for our purposes, is set to 1 to measure how the system deviates from the half-filled-band limit. This approach allows us to analyze the effects of slight perturbations on the system by examining the changes introduced by  $\mathbf{V}_1$  in relation to the original matrix  $\mathbf{V}_0$ .

Therefore, diagonalizing  $\mathbf{V}_0$ , we have the following eigenvalues:

$$v_0^{(0)} = w_{1,1}z, \quad (\text{A3})$$

$$v_1^{(0)} = w_{0,2}, \quad (\text{A4})$$

$$v_2^{(0)} = -w_{0,2}. \quad (\text{A5})$$

From this solution one can clearly verify that  $v_1^{(0)} > v_2^{(0)}$ ; however, we cannot affirm any condition between  $v_0^{(0)}$  and  $v_1^{(0)}$ , since there is no restriction, so one can establish the condition  $v_1^{(0)} = v_0^{(0)}$ ; this would be essential to find the peculiar temperature, as discussed in Sec. III C. The corresponding eigenvectors can be expressed by

$$|u_0^{(0)}\rangle = |\downarrow\rangle, \quad (\text{A6})$$

$$|u_1^{(0)}\rangle = \frac{1}{\sqrt{2}}(|0\rangle + |\uparrow\rangle), \quad (\text{A7})$$

$$|u_2^{(0)}\rangle = \frac{1}{\sqrt{2}}(-|0\rangle + |\uparrow\rangle). \quad (\text{A8})$$

Now let us improve our previous result, thus the first-order correction on the transfer matrix eigenvalues can be obtained perturbatively, resulting in

$$v_0^{(1)} = 0, \quad (\text{A9})$$

$$v_1^{(1)} = \frac{1}{2}(1 + w_{2,2}), \quad (\text{A10})$$

$$v_2^{(1)} = \frac{1}{2}(1 + w_{2,2}). \quad (\text{A11})$$

Here, evidently we have the condition  $v_0^{(1)} < v_1^{(1)} = v_2^{(1)}$ , because  $w_{2,2} > 0$ .

Similarly, the second-order corrections of eigenvalues become

$$v_0^{(2)} = \frac{z(w_{0,1} + w_{1,2})^2}{2[w_{1,1}z - w_{0,2}]} + \frac{z(w_{0,1} - w_{1,2})^2}{2[w_{1,1}z + w_{0,2}]}, \quad (\text{A12})$$

$$v_1^{(2)} = \frac{1}{8} \frac{(w_{2,2} - 1)^2}{w_{0,2}} - \frac{z(w_{0,1} + w_{1,2})^2}{2[w_{1,1}z - w_{0,2}]}, \quad (\text{A13})$$

$$v_2^{(2)} = -\frac{1}{8} \frac{(w_{2,2} - 1)^2}{w_{0,2}} - \frac{z(w_{0,1} - w_{1,2})^2}{2[w_{1,1}z + w_{0,2}]}. \quad (\text{A14})$$

It is evident that  $u_1^{(2)} > u_2^{(2)}$  and  $u_2^{(2)} < 0$ .

Therefore, the corresponding eigenvalues up to order  $\mathcal{O}(\zeta^3)$  are given approximately as follows:

$$\lambda_j = v_j^{(0)} + \zeta v_j^{(1)} + \zeta^2 v_j^{(2)} + \mathcal{O}(\zeta^3). \quad (\text{A15})$$

It is evident that the eigenvalues up to second-order correction indicate that  $\lambda_1 > \lambda_2$ . However, we cannot affirm just by looking at the perturbative eigenvalues which eigenvalue is the largest,  $\lambda_0$  or  $\lambda_1$ , although we have confirmed at the end of Sec. II A that  $\lambda_0$  must be the largest one. Nevertheless, our perturbative result could be useful to find the condition of peculiar temperature up to second-order approximation. Therefore, by using the condition given in (33) we can find the following relation:

$$w_{1,1}z - w_{0,2} + \frac{3(1 + w_{2,2})}{2} - \frac{1}{8} \frac{(w_{2,2} - 1)^2}{w_{0,2}} - \frac{z(w_{0,1} - w_{1,2})^2}{2[w_{1,1}z + w_{0,2}]} = 0. \quad (\text{A16})$$

This result would be relevant when we look for a more accurate value of the peculiar temperature.

- 
- [1] S. M. de Souza and O. Rojas, *Solid State Commun.* **269**, 131 (2018).
- [2] W. Yin, *Phys. Rev. Res.* **6**, 013331 (2024).
- [3] W. Yin, *Phys. Rev. B* **109**, 214413 (2024).
- [4] J. Strečka and K. Karlová, *Eur. Phys. J. B* **97**, 74 (2024).
- [5] J. Chapman, B. Tomasello, and S. T. Carr, [arXiv:2405.20749](https://arxiv.org/abs/2405.20749).
- [6] I. M. Carvalho, J. Torrico, S. M. de Souza, O. Rojas, and O. Derzhko, *Ann. Phys.* **402**, 45 (2019).
- [7] J. Strečka, *Acta Phys. Pol. A* **137**, 610 (2020).
- [8] W. Yin, [arXiv:2401.00948](https://arxiv.org/abs/2401.00948).
- [9] T. Hutak, T. Krokhmalkii, O. Rojas, S. M. de Souza, and O. Derzhko, *Phys. Lett. A* **387**, 127020 (2021).
- [10] W. Yin, [arXiv:2006.15087](https://arxiv.org/abs/2006.15087).
- [11] J. Torrico, M. Rojas, S. M. de Souza, O. Rojas, and N. S. Ananikian, *Europhys. Lett.* **108**, 50007 (2014).
- [12] J. Torrico, M. Rojas, S. M. de Souza, and O. Rojas, *Phys. Lett. A* **380**, 3655 (2016).
- [13] L. Galisova and J. Strečka, *Phys. Rev. E* **91**, 022134 (2015).
- [14] O. Rojas, J. Strečka, and S. M. de Souza, *Solid State Commun.* **246**, 68 (2016).
- [15] J. Strečka, R. C. Alecio, M. Lyra, and O. Rojas, *J. Magn. Magn. Mater.* **409**, 124 (2016).
- [16] O. Rojas, J. Strečka, M. L. Lyra, and S. M. de Souza, *Phys. Rev. E* **99**, 042117 (2019).
- [17] T. Krokhmalkii, T. Hutak, O. Rojas, S. M. de Souza, and O. Derzhko, *Physica A* **573**, 125986 (2021).
- [18] O. Rojas, S. M. de Souza, J. Torrico, L. M. Verissimo, M. S. S. Pereira, and M. L. Lyra, *Phys. Rev. E* **103**, 042123 (2021).
- [19] Y. Panov and O. Rojas, *Phys. Rev. E* **103**, 062107 (2021).
- [20] J. Hubbard, *Proc. R. Soc. London A* **276**, 238 (1963).
- [21] F. H. L. Essler, H. Frahm, F. Göhmann, A. Klümper, and V. E. Korepin, *The One-Dimensional Hubbard Model* (Cambridge University, Cambridge, 2009).
- [22] Z. Wang, D. Psichos, R. F. Badilla, and S. Mazumdar, *J. Phys.: Condens. Matter* **21**, 095009 (2009).
- [23] E. Dagotto and Y. Tokura, *MRS Bull.* **33**, 1037 (2008).

- [24] M. Tsuchiizu and A. Furusaki, *Phys. Rev. B* **69**, 035103 (2004).
- [25] S. Glocke, A. Klümper, and J. Sirker, *Phys. Rev. B* **76**, 155121 (2007).
- [26] P. Sengupta, A. W. Sandvik, and D. K. Campbell, *Phys. Rev. B* **65**, 155113 (2002).
- [27] A. W. Sandvik, L. Balents, and D. K. Campbell, *Phys. Rev. Lett.* **92**, 236401 (2004).
- [28] F. Mila and X. Zotos, *Europhys. Lett.* **24**, 133 (1993).
- [29] H. Ding and J. Zhang, *Chin. J. Phys.* **54**, 237 (2016).
- [30] X. Wang, E. Khatami, F. Fei, J. Wyrick, P. Namboodiri, R. Kashid, A. F. Rigosi, G. Bryant, and R. Silver, *Nat. Commun.* **13**, 6824 (2022).
- [31] H.-X. Wang, Y.-M. Wu, Y.-F. Jiang, and H. Yao, *Phys. Rev. B* **109**, 045102 (2024).
- [32] A. J. Epstein, S. Etemad, A. F. Garito, and A. J. Heeger, *Solid State Commun.* **9**, 1803 (1971).
- [33] R. A. Bari, *Phys. Rev. B* **3**, 2662 (1971).
- [34] G. Beni and P. Pincus, *Phys. Rev. B* **9**, 2963 (1974).
- [35] J. P. Gallinar, *Phys. Rev. B* **11**, 4421 (1975).
- [36] F. Mancini, *Eur. Phys. J. B* **47**, 527 (2005).
- [37] F. Mancini and F. P. Mancini, *Phys. Rev. E* **77**, 061120 (2008).
- [38] F. Mancini and F. P. Mancini, *Eur. Phys. J. B* **68**, 341 (2009).
- [39] R. J. Baxter, *Exactly Solved Models in Statistical Mechanics* (Academic, New York, 1982).
- [40] V. Derzhko and J. Jedrzejewski, [arXiv:1004.2786](https://arxiv.org/abs/1004.2786).
- [41] N. Alves Jr. and C. S. O. Yokoi, *Braz. J. Phys.* **30**, 667 (2000).
- [42] Y. Wang, W. Guo, and H. W. J. Blöte, *Phys. Rev. E* **91**, 032123 (2015).
- [43] O. Rojas, *Braz. J. Phys.* **50**, 675 (2020); *Acta Phys. Pol. A* **137**, 933 (2019).
- [44] R. A. Pimenta, O. Rojas, and S. M. de Souza, *J. Magn. Magn. Mater.* **550**, 169070 (2022).